Biochemical and Biophysical Research Communications 458 (2015) 246–250

Contents lists available at ScienceDirect

Biochemical and Biophysical Research Communications

journal homepage: www.elsevier.com/locate/ybbrc

Structure of the GcpE-HMBPP complex from *Thermus thermophilius*

Ingo Rekittke [a, b], Eberhard Warkentin [b], Hassan Jomaa [a, **], Ulrich Ermler [b, *]

[a] Universitätsklinikum Gießen und Marburg GmbH, Marburg, Germany
[b] Max-Planck-Institut für Biophysik, Frankfurt am Main, Germany

ARTICLE INFO

Article history:
Received 12 January 2015
Available online 7 February 2015

Keywords:
Isoprenoid biosynthesis
GcpE/IspG
HMBPP
X-ray structure
Drug design

ABSTRACT

Isoprenoid biosynthesis in many bacteria, plant chloroplasts and parasitic protozoa but not in humans proceeds via the mevalonate independent 2-C-methyl-D-erythritol-4-phosphate (MEP) pathway. Its penultimate reaction step is catalyzed by (E)-1-hydroxy-2-methyl-but-2-enyl-4-diphosphate (HMBPP) synthase (GcpE/IspG) which transforms 2-C-methyl-D-erythritol-2, 4-cyclo-diphosphate (MEcPP) to HMBPP. In this report we present the structure of GcpE of Thermus thermophiles in complex with its product HMBPP at a resolution of 1.65 Å. The GcpE-HMBPP like the GcpE–MEcPP structure is found in a closed, the ligand-free GcpE structure in an open enzyme state. Imposed by the rigid protein scaffold inside the active site funnel, linear HMBPP and circular MEcPP adopt highly similar conformations. The confined space also determines the conformational freedom of transition state intermediates and the design of anti-infective drugs. The apical Fe of the [4Fe–4S] cluster is coordinated to MEcPP in the GcpE–MEcPP complex and to a hydroxyl/water ligand but not to HMBPP in the GcpE-HMBPP complex. The GcpE-HMBPP structure can be attributed to one step in the currently proposed GcpE reaction cycle.

1. Introduction

Isoprenoids are major constituents of lipids, hormons, vitamins etc. and therefore play an essential role in a large variety of biological processes in all organisms. For their biosynthesis branched C5 units derived from the universal building blocks isopentenyl diphosphate (IPP) and its isomer dimethylallyl diphosphate (DMAPP) are covalently coupled. IPP and DMAPP are formed in humans and animals but also in fungi, archaea and some bacteria via the mevalonate pathway while chloroplasts of plants, most bacteria and parasitic protozoa, however, apply the completely different 2-C-methyl-D-erythritol-4-phosphate (MEP) pathway [1–3] (Fig. 1) for this purpose. The MEP pathway is considered as an attractive target for antimicrobial drugs and herbicides [4,5] and therefore intensively explored [6,7].

GcpE, the penultimate enzyme of the MEP pathway, catalyzes the reductive dehydroxylation reaction of 2-C-methyl-D-erythritol-2,4-cyclo-diphosphate (MEcPP) to (E)-1-hydroxy-2-methyl-but-2-enyl-4-diphosphate (HMBPP) (Fig. 1) [8–10] which is, finally, converted to IPP and DMBPP by (E)-4-hydroxy-3-but-2-enyl-diphosphate reductase (LytB/IspH) [11]. Microbial GcpE has a molecular mass of ca. 44 kDa and plant GcpE of ca. 79 kDa per monomer [8,10,12–14]. Both enzymes contain one [4Fe–4S] cluster which directly participates at the catalytic process (Fig. 1) [15,16]. The complex reaction cycle was studied by EPR spectroscopy, isotope exchange, site-directed mutagenesis, DFT calculations and X-ray crystallography [16–22].

As revealed by an X-ray structure of the Aquifex aeolicus and Thermus thermophilus enzymes [23,24] GcpE is functional as a homodimeric enzyme. Each subunit is composed of a substrate binding N-terminal TIM barrel domain and a C-terminal [4Fe–4S] cluster carrying α/β-domain that are spatially separated and connected by a solvent-exposed linker of five amino acids. The structure of the binary GcpE–MEcPP complex established the mode of substrate binding inside the conserved and positively charged TIM-barrel funnel [25]. Comparison between the empty and substrate-bound GcpE structure revealed an open and closed enzymatic state. MEcPP binding induces a 60° rotation of the α/β-domain onto the TIM-barrel entrance of the partner subunit of the dimer which

* Corresponding author. Max-Planck-Institut für Biophysik, Max-von-Laue-Straße 3, D-60438 Frankfurt, Germany. Fax: +49 69 6303 1002.
** Corresponding author. Universitätsklinikum Gießen und Marburg GmbH, Standort Marburg, Institut für Laboratoriumsmedizin und Pathobiochemie, Baldingerstraße, 35043 Marburg, Germany. Fax: +49 6421 58 65594.
E-mail addresses: Hassan.Jomaa@uk-gm.de (H. Jomaa), ulrich.ermler@biophys.mpg.de (U. Ermler).

http://dx.doi.org/10.1016/j.bbrc.2015.01.088
0006-291X/

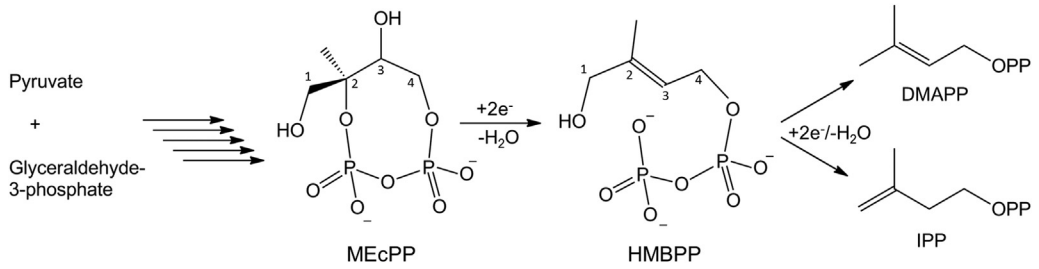

Fig. 1. Reaction of GcpE. 2-C-methyl-D-erythritol 2,4-cyclodiphosphate (MEcPP) is converted to (E)-4-hydroxy-3-methyl-but-2-enyl-diphosphate (HMBPP) by GcpE. The reaction comprises a reductive elimination that causes a ring opening. The produced HMBPP is reduced to the isoprenoid precursors DMAPP and IPP by LytB.

thus largely buries the substrate. During this open-to-closed transition the [4Fe–4S] cluster is displaced ca. 25 Å and one iron ligated to Glu350 in the open state becomes coordinated to the C3 oxygen of MEcPP in the closed state.

Here we report on the structure of GcpE complexed with its product HMBPP, compare the binding mode of HMBPP with that of MEcPP in the GcpE–MEcPP complex and discuss its impact for the mechanism of action and the design of inhibitors.

2. Materials and methods

2.1. Recombinant production and biochemical characterization of GcpE from T. thermophilus

A synthetic gene encoding GcpE of T. thermophilus was cloned into the pQE-60 expression vector and then expressed in TOP10 E. coli cells [10,25]. The [4Fe–4S] cluster was completely incorporated without subsequent reconstitution experiments. Anaerobic purification was achieved by weak anion exchange (DEAE sepharose), strong anion exchange (Source 15Q) and size exclusion chromatography (Superdex 200). The yield was 25 mg enzyme from 9 L cell culture and the enzyme was pure according to SDS-PAGE. GcpE was stored at a concentration of ca. 10 mg/ml in 30 mM Tris–HCl, pH 7.5 and 150 mM NaCl.

2.2. X-ray structure analysis

Crystallization screens were performed under anaerobic conditions at 18 °C using the sitting drop vapor diffusion method combined with a random microseeding strategy [26]. GcpE crystals grown in 30% (v/v) MPD and 20% (v/v) ethanol were used for seed production [24]. The most suitable crystals of GcpE from T. thermophilus grew in 0.6 μL enzyme solution, containing 5 mM HMBPP, and 0.6 μL precipitant composed of 45% pentaerythritol propoxylate 426, 0.1 M MES pH 6.0, 0.4 M KCl, 0.1% NaN_3 (JBScreen Pentaerythritol 1, C6, Jena Bioscience) and 0.1 μL seed stock. Data were collected up to 1.65 Å resolution at the PXII beamline of the Swiss Light Source (Villigen) and processed with XDS [27] (Table 1). The test for merohedral twinning [28] was positive and the initially determined space group $P6_122$ was reduced to $P6_1$. The unit cell parameters were 63.3 Å and 372.1 Å. Phases were determined by the molecular replacement method using Phaser [29] with the structure of the GcpE–MEcPP complex as model [25]. Models were built with Coot [30]. Twin refinement with the operator h,-h-k,-l converges to an R/R_{free} factor of 12.2/17.0% at a resolution range 50.0–1.65 Å using Phenix [31] (Table 1). Figs. 2–4 were produced with PYMOL (Schrödinger, LLC). The atomic coordinates and structure factors of the GcpE-HMBPP complex have been deposited in the Protein Data Bank, www.pdb.org with ID code 4S23.

3. Results and discussion

3.1. The GcpE-HMBPP complex structure

The structure of the GcpE-HMBPP complex at 1.65 Å resolution revealed the substrate HMBPP with a high occupancy (temperature factor of 15 $Å^2$). Its binding mode is virtually identical in both monomers of the asymmetric unit. In contrast to substrate-free GcpE, the GcpE-HMBPP complex is found like the GcpE–MEcPP complex in a closed state [25] (Fig. 2A). The determined structure thus confirms the open-to-close scenario established for the GcpE reaction. Interestingly, the presence of a closed state is not connected with the covalent bond between the [4Fe–4S] cluster and the 3-OH group of MEcPP as HMBPP misses this functional group (Fig. 1). Instead, the apical Fe is coordinated to a hydroxyl/water ligand (Fe–O distance 2.2 Å) (Fig. 2B) which is, in addition, hydrogen-bonded to Asn346-ND2 and Glu232-OE2 in the GcpE-HMBPP structure (Fig. 3). The absence of a covalent Fe-polypeptide/substrate adduct does not imply a (partial) dissociation of the apical Fe in the presence of HMBPP reflected in similar temperature factors of the four irons of the [4Fe–4S] cluster of 12.2, 14.2, 14.4 and 14.0 $Å^2$. Notably, the apical iron of LytB is also protected by its substrate HMBPP but not by its products [32].

The structures of the GcpE–MEcPP and –HMBPP complexes are nearly identical as indicated by an rmsd of 0.4 Å using the C_α atoms for calculation [33]. HMBPP and MEcPP are embedded into the funnel of the TIM barrel domain in a manner that the methylbutenol/methylerythritol part points to the α/β-domain facing the [4Fe–4S] cluster while the diphosphate part is directed to the

Table 1
X-ray analysis statistics.

Data set	GcpE-HMBPP
Data collection	
Wavelength (Å)	0.972
Space group	$P6_1$
Resolution (Å)	1.65 – 50.0 (1.65–1.75)
Cell axis (Å)	63.3, 372.1
Completeness (%)	94.4 (73.6)
R_{sym} (%)	9.0 (38.3)
I/sig(I)	16.7 (2.3)
Redundancy	7.3 (2.1)
Refinement statistics	
No. of monomers in the asymmetric unit	2
No. of residues, [4Fe–4S] cluster, substrate, solvent	2 x 405, 2, 2, 2372
Resolution (Å)	1.65–50.0 (1.65–1.68)
$R_{working}$, R_{free} (%)	12.2, 17.0 (21.4, 30.2)
$B_{average}$ ($Å^2$) polypeptide, [4Fe–4S] cluster, substrate, solvent	15.0, 14.0, 13.6, 28.3
R.m.s. deviation bond lengths (Å)	0.006
bond angles (°)	1.18
Ramachandran Plot favored/allowed/unfavorable (%)	97.8, 2.2, 0.0

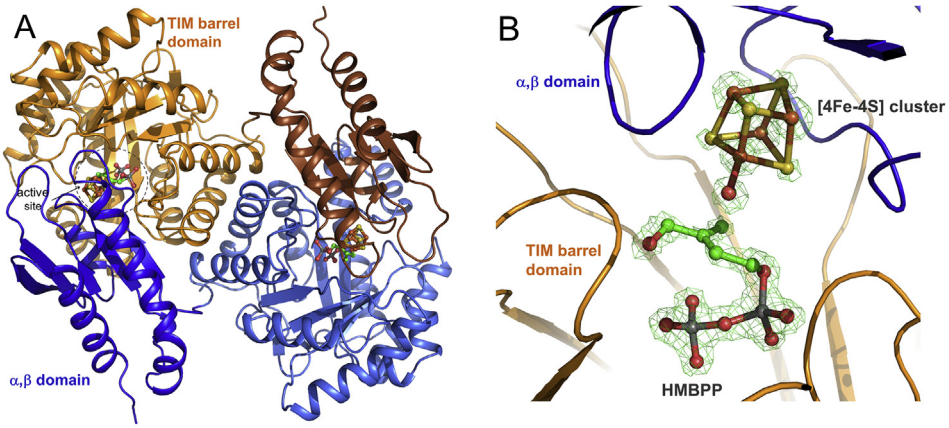

Fig. 2. Structure of the GcpE-HMBPP complex. (A) Overall structure. The TIM barrel and α,β domains of the homodimer (orange, blue) are oriented in a head-to-tail arrangement such that one active site is built up inside a funnel between the substrate and the [4Fe–4S] cluster of the partner subunit. The [4Fe–4S] cluster and HMBPP are shown in a ball-and-stick representation. (B) Active site. The electron densities of the [4Fe -4S] cluster, the hydroxyl/water ligand and HMBPP are contoured at 7.0, 2.2 and 2.2 σ, respectively. In the X-ray structure HMBPP is present in an E-configuration in agreement with the findings of previous NMR studies [8]. A hydroxyl/water (red sphere) is ligated to the apical Fe of the [4Fe–4S] center. Although the [4Fe–4S] cluster remains intact in the presence of HMBPP during the long-term crystallization experiment, the open conformation with the Glu350-ligated Fe represents the stable resting state under physiological conditions [24].

funnel bottom (Fig. 2B). Their positions and conformations are thereby highly similar (Fig. 4).

Linear HMBPP is arranged in a nearly closed hairpin-shaped conformation such that the intramolecular hydrogen bond between its ethanol hydroxyl group and the β-phosphate oxygen formed in MEcPP remains unchanged in HMBPP and the methylbutenol C2 and the β-phosphate oxygen cleaved by the GcpE reaction are still in van der Waals contact to each other (Fig. 4). HMBPP forms exactly the same hydrogen-bond pattern to the polypeptide than MEcPP (Fig. 3) the side chain adjustments being below 0.5 Å. This holds also true for the acidic residues Arg56 and Arg110 involved in compensating the generated negative charge upon ring cleavage [25]. HMBPP inside LytB [32] and the butyrophilin BTN3A1 domain [34] is also arranged in a hairpin-shaped conformation although its curvature becomes smaller and, consequently, the distance between C2 and the oxygen with 4.4 Å and 7.2 Å, respectively, longer compared to a distance of 3.0 Å in GcpE. These conformational variations are mainly due to rotations around the C4-oxygen (linked to α-phosphate) and the C3–C4 bonds.

Nevertheless, minor structural differences between the MEcPP and HMBPP binding mode exists which can be reliably described on the basis of the accurately determined GcpE–MEcPP and –HMBPP structures. The distance ca. 1.5 Å longer between C2 and the β-phosphate oxygen in HMBPP compared with the covalent bond (1.44 Å) in the MEcPP ring results in a shift of 0.7 Å and 1.2 Å of the β-phosphate P and the cleaved O towards the funnel bottom. The methylbutenol part of HMBPP is tilted such that C1 and C2 move 0.5 Å towards the funnel entrance and C3 and C4 ca. 0.9 Å, respectively, towards its bottom compared to MEcPP (Fig. 4). The positions of C3 and C4 are also determined by structural requirements of a double bond between C2 and C3 of HMBPP and by the necessity to evade the hydroxyl/water ligand of the apical Fe (Fig. 2B). In order to adjust a van der Waals distance between HMBPP and the iron ligating hydroxyl/water of ca. 3 Å, the [4Fe–4S] cluster is slightly rotated around its S2 sulfur in the GcpE-HMBPP compared to the GcpE–MEcPP structure resulting in a shift of the apical Fe of 0.5 Å away from C3 of HMBPP (Fig. 4). The distance of the C2–C3

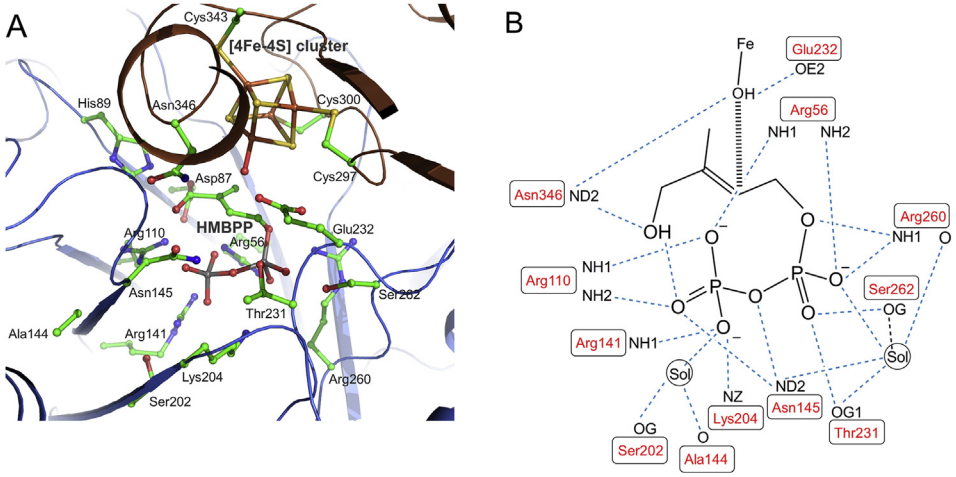

Fig. 3. Hydrogen-bond interactions between GcpE and HMBPP (A) and schematically (B). HMBPP is multiple anchored to the protein scaffold mainly by acidic residues to compensate the negative charge of the biphosphate moiety.

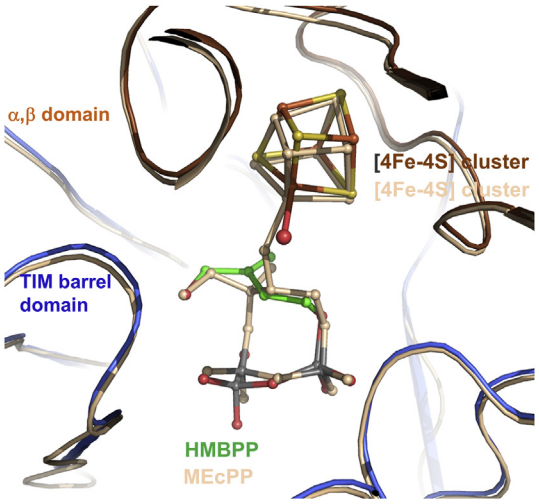

Fig. 4. Superposition of the GcpE–MEcPP and GcpE-HMBPP structures. The circular MEcPP (carbons in salmon) and the linear HMBPP (carbons in green) are found in highly similar conformations.

double bond to the apical iron is 3.9 Å and is thus too far away to form significant π metallacyclic interactions. In the LytB-HMBPP structure the equivalent distance is 3.0 Å [32].

3.2. Implications for catalysis and inhibitor design

The GcpE-HMBPP structure provides various information about the enzymatic mechanism and inhibitor design. In the currently most plausible reaction cycle [7] (see also sFig. 1) the GcpE-HMBPP structure reflects a state after the final elimination reaction and prior to the closed-to-open transition of the $\alpha\beta$ domain which is required to release the product and to return into the open resting state. Obviously, HMBPP can induce an open-to-closed movement and the resulting short-living closed state of GcpE can be trapped (Fig. 2) when using high concentrations of HMBPP and suitable crystallization solutions. Assuming an equilibrium between open and closed states, a GcpE-HMBPP structure in the open state also appears to be feasible when promoted by favorable crystal contacts. No attractive mechanistic scenario about the closed-to-open transition is offered by the available structural data. We assume that the dissociation of the Fe–O3 bond and the strained conformation of the HMBPP contribute to the shift of the equilibrium towards the open state.

Due to the limited space inside the funnel and specifically positioned hydrogen-bond donor/acceptors the structures of the MEcPP ring and the linear HMBPP are highly similar (Fig. 2B + 3). Therefore, it is highly unlikely that intermediates of the reaction cycle are subjected to large rearrangements. Thus, a covalent bond between the 1-OH group and the apical iron can be excluded. According to recent isotope exchange and EPR-spectroscopic data the GcpE reaction proceeds via a carbanionic and a Fe–C2–C3–O3 ferraoxetane-type but presumably not via an epoxide intermediate (see sFig. 1) [16,19–21,35]. Consequently, the Fe–O3 bond remains formed during the entire catalytic cycle until the final elimination process. The proposed organometallic ferraoxetane intermediate might be realized by a tilt around the Fe–O3–C3 bonds. C2 moves towards the [4Fe–4S] cluster in the same direction as described for HMBPP compared with MEcPP (Fig. 4) but the path length is ca. 2 Å prolonged. Interference with the surrounding polypeptide can be avoided by a minor rearrangement of Asn346 and a rotation around the C2 and C3 bond.

The most attractive proton donor for O3 to catalyze the final elimination reaction is the strictly conserved Glu323 which presumably also accepts the proton from the O3 hydroxyl group of MEcPP during its binding in the initial step (sFig. 1). Its hydrogen-bond to the hydroxyl/water ligand of the apical iron underlines this assumed role. The GcpE-HMBPP structure does not offer a plausible clue regarding the essential role of the conserved Asp87-His89 pair demonstrated by mutagenesis studies [23]. A defined water chain between the Asp87-His89 pair in the active site and the protein surface might be necessary as outward channel for surplus water molecules when the α/β-domain enters into the funnel. More detailed mechanistic insights have to await future DFT calculations on the basis of the spectroscopic data [16,22] and the characterized GcpE–MEcPP and –HMBPP structures.

The enzymes of the MEP pathway including GcpE are regarded as promising targets for the rational design of anti-infective drugs and herbicides. HMBPP characterized in the GcpE-HMBPP structure represents the prototype of linear biphosphate containing compounds, one class of potent GcpE inhibitors [18]; thus the detailed knowledge of its binding mode (Fig. 3) can be exploited for the development of inhibitors. The structural data also teaches us that the high affinity of Fe to a hydroxyl/water ligand can prevent the formation of favorable π interactions between the unsaturated bond of the inhibitor and Fe. As a consequence, the interpretation of the EPR data of the GcpE-HMBPP complex in terms of a bio-organometallic bond is challenged by the presented structure. However, the binding of the double/triple bond might vary between different alkenes and alkynes. Thus, the binding mode of HMBPP might be distinct from that of propargyl diphosphate due to the higher affinity to GcpE, the large C13 hyperfine signal in the ENDOR spectrum [18] and the absence of bulky methyl and ethanol substituents of the latter. An optimal geometry for strong π η^2-alkenyl interactions appears to be only feasible when the double/triple bond starts at the carbon next to that linked to diphosphate. The limited space inside the active site funnel only allows the application of small substituents (except for the diphosphate) at the carbons of the double/triple bond (Fig. 3).

Conflict of interest

None.

Acknowledgments

This work was supported by the Else Kröner-Fresenius-Stiftung and the Max-Planck Society. We thank Hartmut Michel for continuous support and the staffs of PXII at the Swiss Light Source (Villigen) for help during data collection.

Appendix A. Supplementary data

Supplementary data related to this article can be found at http://dx.doi.org/10.1016/j.bbrc.2015.01.088.

Transparency document

Transparency document related to this article can be found online at http://dx.doi.org/10.1016/j.bbrc.2015.01.088.

References

[1] S. Horbach, H. Sahm, R. Welle, Isoprenoid biosynthesis in bacteria: two different pathways? FEMS Microbiol. Lett. 111 (1993) 135–140.
[2] G.A. Sprenger, U. Schorken, T. Wiegert, S. Grolle, A.A. de Graaf, S.V. Taylor, T.P. Begley, S. Bringer-Meyer, H. Sahm, Identification of a thiamin-dependent synthase in Escherichia coli required for the formation of the 1-deoxy-D-

xylulose 5-phosphate precursor to isoprenoids, thiamin, and pyridoxol, Proc. Natl. Acad. Sci. U S A 94 (1997) 12857–12862.
[3] M. Rohmer, From molecular fossils of bacterial hopanoids to the formation of isoprene units: discovery and elucidation of the methylerythritol phosphate pathway, Lipids 43 (2008) 1095–1107.
[4] M. Rohmer, C. Grosdemange-Billiard, M. Seemann, D. Tritsch, Isoprenoid biosynthesis as a novel target for antibacterial and antiparasitic drugs, Curr. Opin. Investig. Drugs 5 (2004) 154–162.
[5] J. Wiesner, H. J, Isoprenoid biosynthesis of the apicoplast as drug target, Curr. Drug Targets 8 (2007) 3–13.
[6] T. Grawert, M. Groll, F. Rohdich, A. Bacher, W. Eisenreich, Biochemistry of the non-mevalonate isoprenoid pathway, Cell. Mol. Life Sci. 68 (2011) 3797–3814.
[7] W. Wang, E. Oldfield, Bioorganometallic chemistry with IspG and IspH: structure, function, and inhibition of the [Fe(4)S(4)] proteins involved in isoprenoid biosynthesis, Angew. Chem. Int. Ed. Engl. 53 (2014) 4294–4310.
[8] S. Hecht, W. Eisenreich, P. Adam, S. Amslinger, K. Kis, A. Bacher, D. Arigoni, F. Rohdich, Studies on the nonmevalonate pathway to terpenes: the role of the GcpE (IspG) protein, Proc. Natl. Acad. Sci. U S A 98 (2001) 14837–14842.
[9] M. Seemann, B.T. Bui, M. Wolff, D. Tritsch, N. Campos, A. Boronat, A. Marquet, M. Rohmer, Isoprenoid biosynthesis through the methylerythritol phosphate pathway: the (E)-4-hydroxy-3-methylbut-2-enyl diphosphate synthase (GcpE) is a [4Fe-4S] protein, Angew. Chem. Int. Ed. Engl. 41 (2002) 4337–4339.
[10] A.K. Kollas, E.C. Duin, M. Eberl, B. Altincicek, M. Hintz, A. Reichenberg, D. Henschker, A. Henne, I. Steinbrecher, D.N. Ostrovsky, R. Hedderich, E. Beck, H. Jomaa, J. Wiesner, Functional characterization of GcpE, an essential enzyme of the non-mevalonate pathway of isoprenoid biosynthesis, FEBS Lett. 532 (2002) 432–436.
[11] F. Rohdich, S. Hecht, K. Gartner, P. Adam, C. Krieger, S. Amslinger, D. Arigoni, A. Bacher, W. Eisenreich, Studies on the nonmevalonate terpene biosynthetic pathway: metabolic role of IspH (LytB) protein, Proc. Natl. Acad. Sci. U S A 99 (2002) 1158–1163.
[12] J. Querol, N. Campos, S. Imperial, A. Boronat, M. Rodriguez-Concepcion, Functional analysis of the Arabidopsis thaliana GCPE protein involved in plastid isoprenoid biosynthesis, FEBS Lett. 514 (2002) 343–346.
[13] M. Seemann, P. Wegner, V. Schunemann, B.T. Bui, M. Wolff, A. Marquet, A.X. Trautwein, M. Rohmer, Isoprenoid biosynthesis in chloroplasts via the methylerythritol phosphate pathway: the (E)-4-hydroxy-3-methylbut-2-enyl diphosphate synthase (GcpE) from Arabidopsis thaliana is a [4Fe-4S] protein, J. Biol. Inorg. Chem. 10 (2005) 131–137.
[14] Y.L. Liu, F. Guerra, K. Wang, W. Wang, J. Li, C. Huang, W. Zhu, K. Houlihan, Z. Li, Y. Zhang, S.K. Nair, E. Oldfield, Structure, function and inhibition of the two- and three-domain 4Fe-4S IspG proteins, Proc. Natl. Acad. Sci. U S A 109 (2012) 8558–8563.
[15] D. Adedeji, H. Hernandez, J. Wiesner, U. Kohler, H. Jomaa, E.C. Duin, Possible direct involvement of the active-site [4Fe-4S] cluster of the GcpE enzyme from thermus thermophilus in the conversion of MEcPP, FEBS Lett. 581 (2007) 279–283.
[16] W. Wang, K. Wang, J. Li, S. Nellutla, T.I. Smirnova, E. Oldfield, An ENDOR and HYSCORE investigation of a reaction intermediate in IspG (GcpE) catalysis, J. Am. Chem. Soc. 133 (2011) 8400–8403.
[17] F. Rohdich, F. Zepeck, P. Adam, S. Hecht, J. Kaiser, R. Laupitz, T. Grawert, S. Amslinger, W. Eisenreich, A. Bacher, D. Arigoni, The deoxyxylulose phosphate pathway of isoprenoid biosynthesis: studies on the mechanisms of the reactions catalyzed by IspG and IspH protein, Proc. Natl. Acad. Sci. U S A 100 (2003) 1586–1591.
[18] W. Wang, J. Li, K. Wang, C. Huang, Y. Zhang, E. Oldfield, Organometallic mechanism of action and inhibition of the 4Fe-4S isoprenoid biosynthesis protein GcpE (IspG), Proc. Natl. Acad. Sci. U S A 107 (2010) 11189–11193.
[19] W. Xu, N.S. Lees, D. Adedeji, J. Wiesner, H. Jomaa, B.M. Hoffman, E.C. Duin, Paramagnetic intermediates of (E)-4-hydroxy-3-methylbut-2-enyl diphosphate synthase (GcpE/IspG) under steady-state and pre-steady-state conditions, J. Am. Chem. Soc. 132 (2010) 14509–14520.
[20] R.L. Nyland 2nd, Y. Xiao, P. Liu, C.L. Meyers, IspG converts an epoxide substrate analogue to (E)-4-hydroxy-3-methylbut-2-enyl diphosphate: implications for IspG catalysis in isoprenoid biosynthesis, J. Am. Chem. Soc. 131 (2009) 17734–17735.
[21] Y. Xiao, D. Rooker, Q. You, C.L. Meyers, P. Liu, IspG-catalyzed positional isotopic exchange in methylerythritol cyclodiphosphate of the deoxyxylulose phosphate pathway: mechanistic implications, Chembiochem 12 (2011) 527–530.
[22] W. Xu, N.S. Lees, D. Hall, D. Welideniya, B.M. Hoffman, E.C. Duin, A closer look at the spectroscopic properties of possible reaction intermediates in wild-type and mutant (E)-4-hydroxy-3-methylbut-2-enyl diphosphate reductase, Biochemistry 51 (2012) 4835–4849.
[23] M. Lee, T. Grawert, F. Quitterer, F. Rohdich, J. Eppinger, W. Eisenreich, A. Bacher, M. Groll, Biosynthesis of isoprenoids: crystal structure of the [4Fe-4S] cluster protein IspG, J. Mol. Biol. 404 (2010) 600–610.
[24] I. Rekittke, T. Nonaka, J. Wiesner, U. Demmer, E. Warkentin, H. Jomaa, U. Ermler, Structure of the E-1-hydroxy-2-methyl-but-2-enyl-4-diphosphate synthase (GcpE) from thermus thermophilus, FEBS Lett. 585 (2011) 447–451.
[25] I. Rekittke, H. Jomaa, U. Ermler, Structure of the GcpE (IspG)-MEcPP complex from thermus thermophilus, FEBS Lett. 586 (2012) 3452–3457.
[26] P.D. Shaw Steward, S.A. Kolek, R.A. Briggs, N.E. Chayen, P.F.M. Baldock, Randow Microseeding: a theoretical and practical exploration of seed stability and seeding techniques for successful protein crystallization, Cryst. Growth & Des. 11 (2011) 3432–3441.
[27] W. Kabsch, Xds, Acta. Crystallogr. D. Biol. Crystallogr. 66 (2010) 125–132.
[28] A.A. Lebedev, A.A. Vagin, G.N. Murshudov, Intensity statistics in twinned crystals with examples from the PDB, Acta Crystallogr. D. Biol. Crystallogr. 62 (2006) 83–95.
[29] A.J. McCoy, R.W. Grosse-Kunstleve, P.D. Adams, M.D. Winn, L.C. Storoni, R.J. Read, Phaser crystallographic software, J. Appl. Crystallogr. 40 (2007) 658–674.
[30] P. Emsley, K. Cowtan, Coot: model-building tools for molecular graphics, Acta Crystallogr. D. Biol. Crystallogr. 60 (2004) 2126–2132.
[31] P.V. Afonine, R.W. Grosse-Kunstleve, V.B. Chen, J.J. Headd, N.W. Moriarty, J.S. Richardson, D.C. Richardson, A. Urzhumtsev, P.H. Zwart, P.D. Adams, phenix.model_vs_data: a high-level tool for the calculation of crystallographic model and data statistics, J. Appl. Crystallogr. 43 (2010) 669–676.
[32] T. Grawert, I. Span, W. Eisenreich, F. Rohdich, J. Eppinger, A. Bacher, M. Groll, Probing the reaction mechanism of IspH protein by x-ray structure analysis, Proc. Natl. Acad. Sci. U S A 107 (2010) 1077–1081.
[33] L. Holm, P. Rosenstrom, Dali server: conservation mapping in 3D, Nucleic Acids Res. 38 (2010) W545–W549.
[34] S. Vavassori, A. Kumar, G.S. Wan, G.S. Ramanjaneyulu, M. Cavallari, S. El Daker, T. Beddoe, A. Theodossis, N.K. Williams, E. Gostick, D.A. Price, D.U. Soudamini, K.K. Voon, M. Olivo, J. Rossjohn, L. Mori, G. De Libero, Butyrophilin 3A1 binds phosphorylated antigens and stimulates human gammadelta T cells, Nat. Immunol. 14 (2013) 908–916.
[35] Y. Xiao, R.L. Nyland 2nd, C.L. Meyers, P. Liu, Methylerythritol cyclodiphosphate (MEcPP) in deoxyxylulose phosphate pathway: synthesis from an epoxide and mechanisms, Chem. Commun. (Camb) 46 (2010) 7220–7222.